Friction stir welding of AISI 316LN high strength austenitic stainless steel for cryogenic application

I Aviles Santillana[1], J Debeux[1], M Meyer[1], M Muddamallappa[2], A Polo Picazo[1], H Robe[3], E Rodriguez Castro[1,4], S Sgobba[1], KP Weiss[5]

[1]*CERN, CH-1211 Genève – Switzerland*
[2]*Texas A&M University. 400 Bizzell Street. College Station, 77843, Texas, United States*
[3] *Institut de Soudure, 4 rue Pilâtre de Rozier, 57420 Goin – France*
[4] *University Carlos III of Madrid, Campus Leganes, Av. Universidad 30, 28911 Madrid – Spain*
[5] *KIT, Institute for Technical Physics, 76344 Eggenstein-Leopoldshafen / Germany*

E-mail: Ignacio.Aviles.Santillana@cern.ch

Abstract. Friction stir welding (FSW) is a solid state joining process that uses the heat generated by the friction of a rotating tool and the base material to join materials together. Due to the fact that the material is never melted, and that extensive plastic deformation is introduced in the weld seam, a unique set of properties is achieved. The technique has been extensively used to join aluminium and aluminium alloys, but very few developments are reported on high strength austenitic stainless steel, which is the material of choice for many high energy physics and fusion magnets. This paper contains a comprehensive microstructural and mechanical characterization, including at cryogenic temperature, of an 8 mm thick high strength austenitic stainless steel plates. The steel grade is the high alloy version of AISI 316LN (identified as 1.4429 or -X2CrNiMoN17-13-3 according to European standards). Special attention was given to cryogenic elastic – plastic J – integral testing of the weld seam. To the authors' knowledge, this is the first time fracture toughness at cryogenic temperature on friction stir welded 1.4429 has been measured.

1. Introduction

Austenitic stainless steel is an excellent material of choice for structural cryogenic applications, thanks to a unique combination of strength, ductility, and toughness at service temperature. Furthermore, it is also a very appealing material for superconducting high field magnets thanks to the very low magnetic permeability of the austenitic phase.

At the European Organization for Nuclear Research (CERN), for its flagship project, High Luminosity LHC (HL-LHC), a series of high field magnets will be integrated in the machine [1]. For the new high field dipoles and quadrupoles, an important component is the cold mass vessel, composed of the shrinking cylinder and the end covers. The vessel is fabricated by welded nitrogen strengthened austenitic stainless steel components, consisting of half shells and covers to be joined together by longitudinal and circular butt welds [2] in order to guarantee an excellent mechanical performance at cryogenic temperature.

This work is intended for the circular welds of the vessel; however, the obtained results show a great potential for any nitrogen strengthened austenitic stainless steel joint, intended for use in cryogenic applications.

1.1. *Friction stir welding of austenitic stainless steel*

Friction Stir Welding (FSW) is a solid-state welding process where a non-consumable rotating tool inserted into the material to be welded creates friction and large plastic deformations to generate heating and softening of the material. During tool movement along the welding line, complex material flow occurs at a temperature below the melting point. FSW involves low heat input and process temperature,

thus avoiding classical fusion weld imperfections such as hot cracking, lack of fusion and porosities, resulting in in a high performance and low distortion weld. Compared to light alloys (aluminium, magnesium…), FSW of hard material or high melting temperature like steels, stainless steels and nickel-based alloys is more difficult due to the temperature to be reached to perform the operations. For these materials, welding temperature is often considered above 1000°C [3] and FSW tool lifetime (i.e., tool wear) is a major issue. Tool must have high abrasion resistance, toughness, and creep resistance at elevated temperature and under high load [4].

In the last two decades, FSW of austenitic stainless steel (mainly AISI 304) has been studied [5 - 9], but only a few very recent publications are found for high N grades [9, 10]. The technique has been used for crack repair [5], grain refinement of fusion welds and more rarely for real part applications. The welding parameters for austenitic stainless steel are quite different than for light and high conducting materials such as aluminium alloys, and imply a low rotation speed, a low welding speed and a high axial force [6].

2. Materials and methods

2.1. *Raw – material specification*

The material which was chosen for the development of friction stir welding is the material which is currently used for the vessels of the 11 T dipoles: the high alloy version of AISI 316LN (1.4429 or X2CrNiMoN17-13-3). This alloy guarantees a fully austenitic microstructure and is very stable against undesired martensitic transformation.

Moreover, the material has been purchased according to CERN's technical specification for ultra – high vacuum (UHV) components [10]. The stringent requirements of this material specification for products intended for UHV purposes, impose to apply an adapted metallurgy and manufacturing process, aimed at meeting the structure and inclusion limits specified. The process shall include a mandatory ElectroSlag Remelting (ESR) step in order to guarantee very stringent requirements of inclusion content according to method D of ASTM E45 (severity level number shall be at most 1).

Additional requirements on the chemical composition are imposed with respect to EN 10028-7 for Ni, Cr, Mo, Co and N, and especially low P and S content are requested. The product analysis can be found in Table 1:

Table 1. Product analysis of the 8 mm plates used as base material. R stands for remainder.

Element	C	S	N	Cr	Ni	Mn	Si	Mo	P	Co	B	Fe
Weight %	0.010	< 0.002	0.19	17.32	13.05	1.34	0.26	2.60	0.024	0.10	0.002	R

The relative magnetic permeability at room temperature after solution annealing shall be lower than or equal to 1.005 for fields of over 80 000 A/m.

The internal soundness and microstructural homogeneity of the 8 mm thick plates used as base material is guaranteed by the ultrasonic examination of 100% of the volume.

2.2. *FSW welding*

With this base material, the FSW specimens were produced using a specific FSW machine (MTS I-STIR 10). The process parameters of this study were determined after several preliminary trials, and they are the following: rotation speed: 125 rev/min; Welding speed: 50 mm/min; Tilt angle: 1.5 degrees; Axial force: 62 kN. The welding operations were conducted in force control only to ensure the stability and quality along the weld. Pure Argon was used as shielding gas to protect both the welding area and the tool from oxidation. The process was performed using a polycrystalline cubic boron nitride (PcBN) tool and a cooled head. The tool was composed of an 8 mm pin length of and a convex 25 mm diameter shoulder, as shown in Figure 1.

Figure 1. Friction stir welding tool (70% PcBN/30% W-Re), with a 8 mm long conical pin and 25 mm diameter convex shoulder.

2.3. *Metallographic examination*

Detailed metallographic observations were performed at several cross sections of the FSW. An example of a macroscopic observation is shown in **Figure *2***, together with a schematic description of the different regions of a FSW, containing the naming convention that will be used to refer to the different regions.

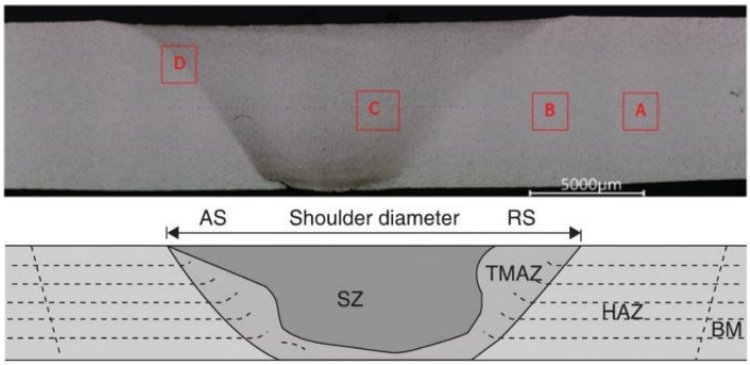

Figure 2. Top) cross section of FSW. Positions marked with letters A – D are the regions where the metallographic observations were carried out. Bottom) schematic of the different regions of a FSW: Advancing side (AS), Retreating side (RS), Stirred zone (SZ), Thermo mechanically affected zone (TMAZ), Heat affected zone (HAZ), Base metal (BM).

Full cross sections were mounted in cold resin, ground and polished down to 1 µm diamond paste. The samples were observed under optical microscope, after chemical etching (Nital® 5% and 10% oxalic acid (etchants #74 and #13b according to the ASTM E407 respectively)). Grain size assessment was done according to ASTM E112, using the linear intercept procedure.

2.4. *Hardness*

A matrix of 7 x 148 Vickers hardness indents (HV2) was performed at a cross section of the FSW. In order to respect the guidelines of ISO 6807 – 1, the distance between indents is 1 mm in thickness and 0.5 mm in the horizontal direction

2.5. *Tensile testing*

Transverse tensile tests were performed in 5 specimens. The geometry and the test parameters are according to ISO 6892-1. The thickness is 6.6 mm (1 mm is removed from the root and 0.4 mm from the face) in order to include as much as possible, the whole cross section of the weld.

Additionally, six flat tensile specimens were extracted according to ISO 6892-4 (gage length: 25 mm; thickness: 3 mm) and have been tested at 4.2 K following the test procedure described in the same standard. They have all been welded via FSW, with the welded zone localized in the middle of the specimen's calibrated length. Thus, transverse tensile tests were performed. Two specimens were extracted from the top (H1 and H2), two from the bottom (B1 and B2) and two at mid-thickness (M1 and M2). 1 mm was removed from the top and the bottom surfaces of the welded coupon before sample extraction to avoid variations in the cross section as well as the contamination observed in 3.1.1.

2.6. *Fracture toughness testing*

Fracture toughness tests were performed on six stainless steel 316LN 6 mm thick compact specimens (T-L orientation) according to ASTM-E1820 at 4 K. As for the tensile specimens, 1 mm was removed from the top and the bottom surfaces of the welded coupon before sample extraction to avoid variations in the cross section as well as the contamination observed in 3.1.1. Three specimens (BM1 – BM3) were extracted from the base material (to be used as a reference), and three specimens (S1 – S3) were extracted with the tip of the notch centred in the FSW's axis (thus, crack growth takes place at the weld bead, as it is shown in Figure 3).

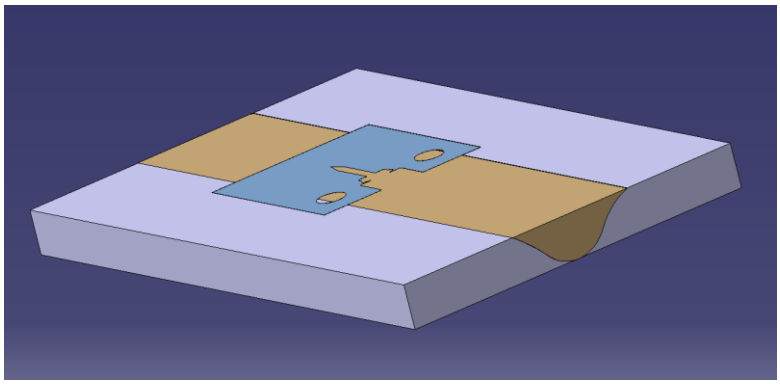

Figure 3. Schematic showing the position of the 'S' specimens with respect to the FSW plates.

An example of a tested specimen as well as the crack opening displacement (COD) gage used to estimate crack growth can be seen in Figure 4. Due to the very high values of toughness expected, at least for the base material [11], an elastic – plastic fracture mechanics' test protocol was put in place: J – tests, single specimen method with the unloading compliance technique for crack estimation. Following the guidelines given by ASTM E1820, after precracking, side grooves were introduced in order to minimize crack deviation and tunnelling.

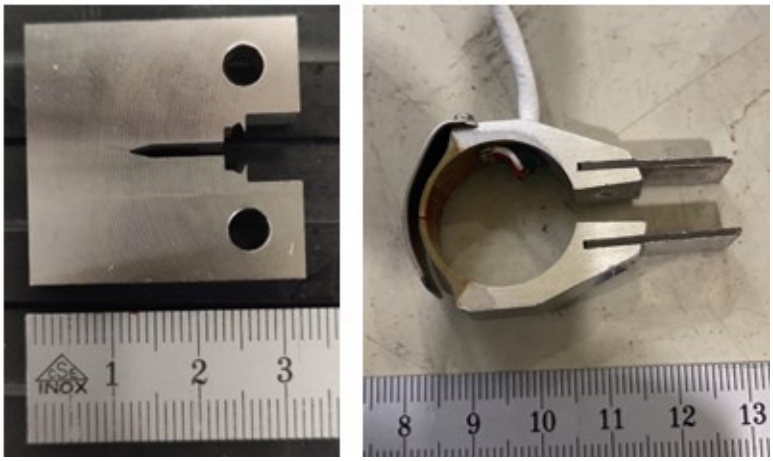

Figure 4. Left) CT specimen after pre cracking. Right) COD gage, courtesy of NHMFL.

3. Results and discussion

3.1. *Weld characterization*

A comprehensive characterization of the weld was performed via metallographic observations and hardness profiles of its cross section:

3.1.1. *Metallographic observations.* As it can be seen in the images below, Figure 5A and Figure 5B, taken at the base metal and heat affected zone respectively, grain size numbers are identical (G = 5) and grains are quite equiaxial. At the SZ, very fine (G = 13) and equiaxial grains are observed (Figure 5C), showing a significant grain refinement due to the FSW process. This effect is observed in Figure 5D, with the transition from the TMAZ and the SZ. The TMAZ corresponds to the area where the deformation and temperature are too low to induce a full recrystallization, thus it is characterized by reoriented and slightly elongated grains due to the shearing efforts introduced by the rotating tool.

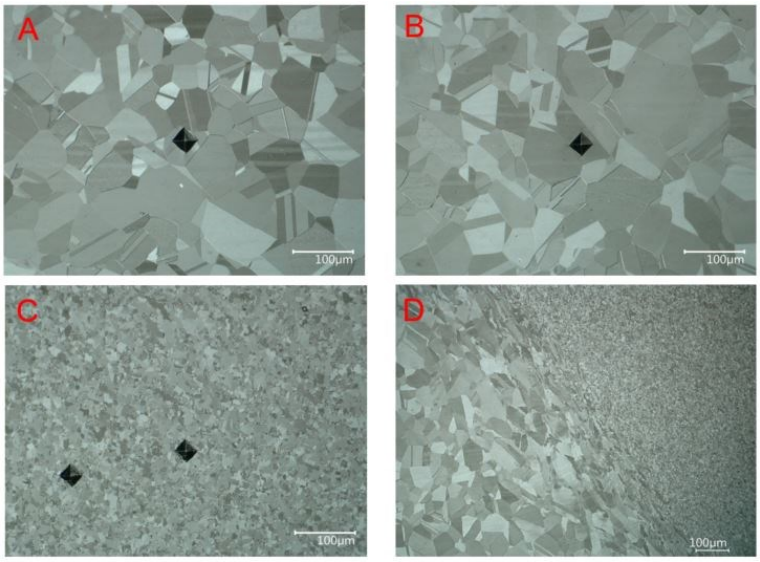

Figure 5. Metallographies selected positions of the FSW. Original magnification: 500x. Some of them contain Vickers indentations. A) Base material; B) HAZ; C)SZ; D) transition between TMAZ and SZ.

Additionally, when looking closer at the weld's root left side, there seems to be a heterogeneity as well as a banded structure. These features were analysed as polished (Figure 6 left) and after Nital® etching (Figure 6 right).

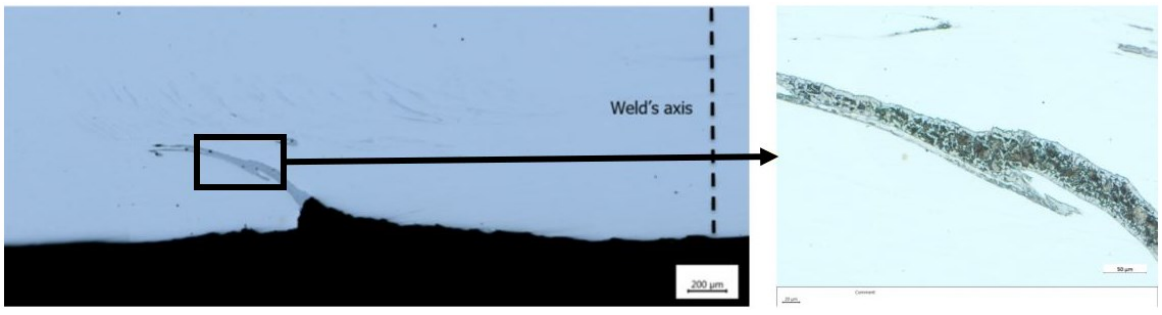

Figure 6. Left) as polished root of the SZ (AS) of FSW. Right) Feature in the orange rectangle. After Nital®. Perlitico – ferritic structure.

Some of them reveal a perlitic – ferritic microstructure, corresponding with inclusions transferred to the weld bead from the anvil used for the FSW. Other secondary phases that did not show any reaction to the etching are most likely a small quantity of δ – ferrite and / or σ – phase. Park et al. already observed (for AISI 304) the formation of these two secondary phases in the advancing side, at the root of the SZ, from introduction of high strain and dynamic recrystallization during FSW [11].

3.1.2. *Hardness profiles*. In order to construct the hardness mapping shown in Figure 7 based on the hardness matrix that was performed, a bilinear interpolation was applied.

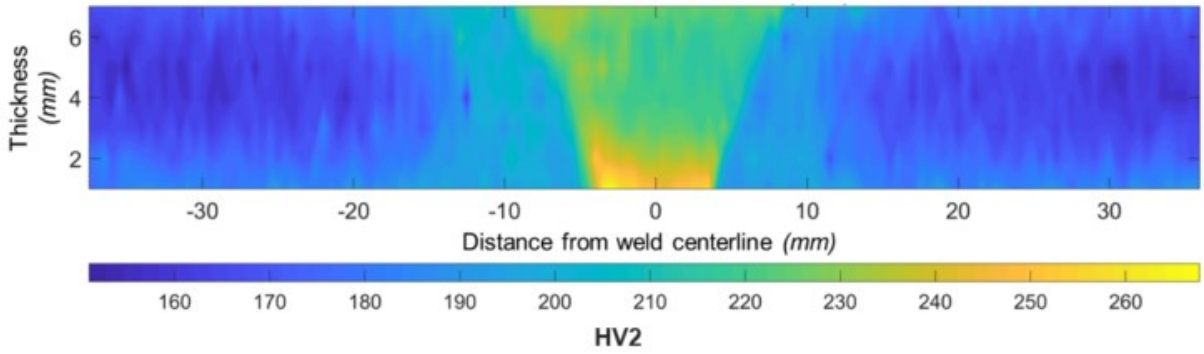

Figure 7. Hardness (HV2) mapping of FSW cross section.

From it, we can observe that all the stirred zones exhibit higher hardness than the base material, induced mainly by a Hall – Petch effect. The highest value of hardness is reached in the centre of the weld's axis, at the nugget. The material hardness changes in the thickness, with the highest values reached at the top and bottom surfaces, where the cooling rate is expected to be higher than at other regions and where extreme grain refinement was observed (see Figure 8). The hardness then decreases in function of the distance from the weld centre line, until it reaches the asymptotic value of the base material at +/- 15mm from the weld's axis. A relatively narrow HAZ is observed, with a similar width on both side of the weld creating a smooth transition to the base metal.

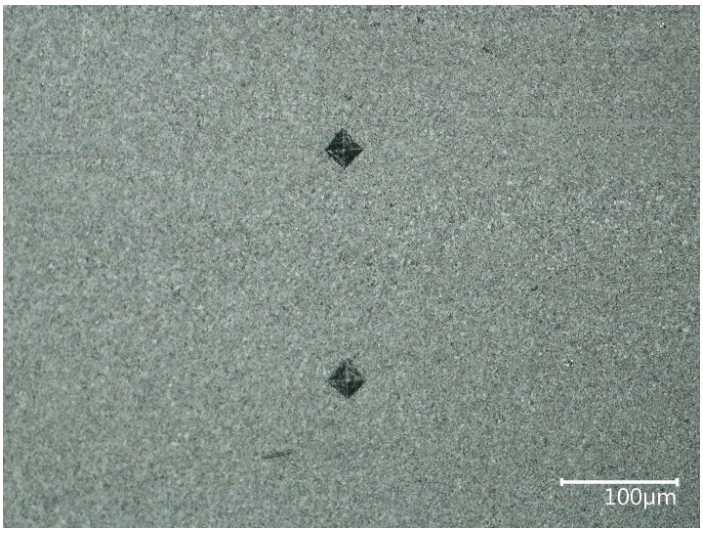

Figure 8. Root of SZ. Original magnification 500x. Vickers indentations are observed. Ultra – fine grain (G=16) is measured.

3.2. *Mechanical testing*
A comprehensive characterization of the FSW was performed, both at room and cryogenic temperatures. At room temperature, tests were performed at the Institut de Soudure (FR) and at cryogenic temperature, tests were performed at CERN (CH).

3.2.1. *Room temperature*. The results of the transverse tensile tests show a joint efficiency > 1 for all the tested specimens (tensile strength is well above the minimum specified value of the parent material; moreover, yield strength is also above the minimum specified value), with the position of the failure always found outside the weld bead and heat affected zone.

3.2.2. *Cryogenic temperature (4.2 K).* Transverse tensile tests and fracture toughness (J – tests) were performed. A detailed analysis of the obtained results is performed here:

Tensile tests results for each specimen are shown in Table 2. Elongation at break is shown for information (the calibrated length is obviously heterogeneous) to highlight the elevated ductility of the specimens at low temperature. For specimen B1, only the tensile strength is shown due to the sliding of the extensometer.

Table 2. Transverse tensile tests results (0.2% proof strength (Rp02); Tensile strength (Rm)and elongation after fracture (A)) of FSW specimens at 4 K

Specimen	Rp_{02} [MPa]	Rm [MPa]	A [%]
H1	1166.3	1483.7	14.6
H2	1190.0	1522.8	16.5
M1	1170.2	1518.1	13.0
M2	1170.2	1530.3	14.5
B1	-	1481.4	-
B2	1153.1	1479.6	16.7

As it can be seen in Table 2, the tensile results show a limited spread of cryogenic tensile properties. Since all the specimens broke well outside the heat affected zone of the weld the joint's strength shows to be higher than the one of the base material.

Figure 9 shows an example of two resistance J - R curves: one obtained for the base material (BM2, left) and one obtained for the FSW (S2, right). They contain all the construction, exclusion and auxiliary lines required for the assessment of J_Q.

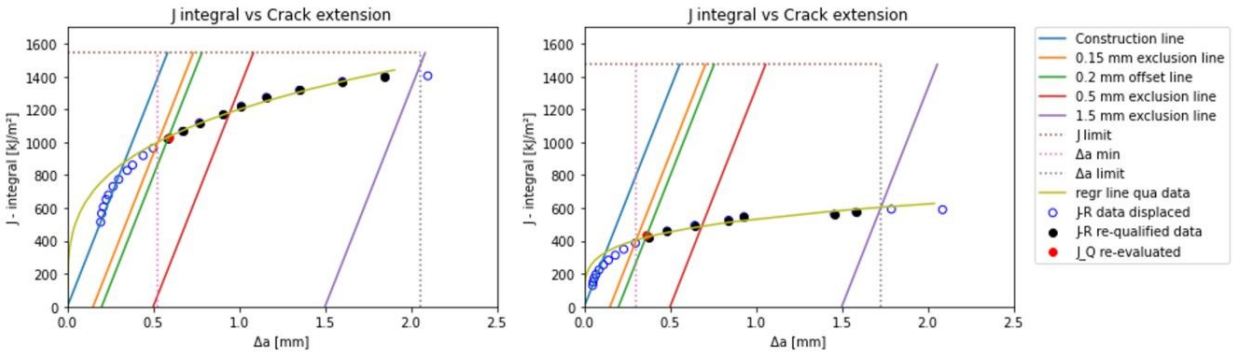

Figure 9. Resistance (J-R) curves. Left) Specimen BM2. Right) Specimen S2.

After crack opening and assessment of the geometrical criteria, only specimen S1 did not fulfil the crack extension requirements of ASTM E1820 due to crack deviation. Thus, the results for this

specimen are not exploitable and are not included. For the other 5 specimens, post processing of the data was performed according to [12], even if there is practically no negative crack extension for any of the tested specimens. J values were recalculated using the corrected crack extension values, and K_{JIC} values were calculated from the J_{IC} values. The results are gathered in Table 3:

Table 3. Fracture toughness at cryogenic temperature results

Specimen	BM1	BM2	BM3	S2	S3
J_{IC} [kJ/m^2]	883	1030	732	442	417
K_{JIC} [MPa√m]	430	465	392	304	296

For each group of specimens, the spread is small, showing a high reproducibility of the results. When comparing the average values for each group of specimens (430 ± 13 MPa√m for the base material, 300 ± 5 MPa√m for the FSW) we see a significant drop of fracture toughness, which can be considered as normal for two reasons: one is the typically higher content of inclusions that can act as crack initiators / stress concentrators as suggested by Morris [13]. The second one is the fact that, based on the obtained results of hardness (see 3.2.2) and tensile tests at cryogenic temperature, higher mechanical properties would be expected at the weld seam (including yield strength). It is known that the relationship between fracture toughness and yield strength for a given material in inversely proportional [14], thus explaining the drop of fracture toughness in the weld seam.

However, based on the obtained results, FSW shows higher fracture toughness values at 4 K than similar joints (same base material) performed by fusion welding (Tungsten Inert Gas) as it can be seen in [15], where values of 262 MPa√m were obtained using 1.4453 as filler material and 266 MPa√m when the filler was JK2LB. The reasons behind can be linked to the inherent nature of the FSW explained above: a solid solution joining technique with low heat input. This will be translated in absence of solidification microcracking and other classical fusion welding imperfections, and less propensity to high temperature secondary phases, detrimental for fracture toughness at cryogenic temperature due to its brittleness [15].

4. Summary and Conclusions

Two 8 mm thick high nitrogen AISI 316LN (1.4429) plates have been successfully joined using FSW. Tensile tests at room temperature already showed a welding efficiency larger than 1. Additionally, a comprehensive metallurgical and mechanical cryogenic assessment of the weld coupon was successfully carried out.

The metallurgical assessment and hardness profiles show that the maximum hardness is achieved at the weld's axis, in the top and bottom surface. At these positions, the most pronounced grain refinement is observed, showing a clear Hall – Petch contribution to the hardness. Hardness values at the HAZ seem to have a thermo – mechanical origin. In the TMAZ, there is a combined effect of both contributions.

Transverse tensile tests at 4 K show high yield and tensile strengths. The rupture occurring always outside the welded zone and far from the heat affected zone confirms what was already observed in the hardness profiles: a significant increase of tensile strength of the FSW compared to the base material.

Fracture toughness tests at 4 K of the FSW were successfully performed for the first time in a high nitrogen AISI 316LN (1.4429). Higher values with respect to more conventional fusion welding techniques have been measured, confirming the excellent mechanical performance of the welded joint. Attention should be taken with the contamination observed at the welds' root by transfer from the anvil and from suspected secondary phases, which can have an impact both in the mechanical and the magnetic performance of the FSW.

5. References

[1] Brüning, O., & Rossi, L. (2019). The high-luminosity large hadron collider. Nature Reviews Physics, 1(4), 241-243.
[2] Brüning, O., et al. High-Luminosity Large Hadron Collider (HL-LHC). 2020.
[3] C. D. Sorensen et T. W. Nelson, Friction Stir Welding of Ferrous and Nickel Alloys, Friction Stir Welding and Processing, p. 10.
[4] M. Almoussawi, A. J. Smith, et M. Faraji, Wear of Polycrystalline Boron Nitride Tool During the Friction Stir Welding of Steel, Metallography, Microstructure, and Analysis, vol. 7, no 3, p. 252-267, juin 2018, doi: 10.1007/s13632-018-0439-0.
[5] C. Gunter, M. P. Miles, F. C. Liu, et T. W. Nelson, Solid state crack repair by friction stir processing in 304L stainless steel, Journal of Materials Science & Technology, vol. 34, no 1, p. 140-147, janv. 2018, doi: 10.1016/j.jmst.2017.10.023.
[6] A. P. Reynolds, W. Tang, T. Gnaupel-Herold, et H. Prask, Structure, properties, and residual stress of 304L stainless steel friction stir welds, Scripta Materialia, vol. 48, no 9, p. 1289-1294, mai 2003, doi: 10.1016/S1359-6462(03)00024-1.
[7] S. H. C. Park, *et al.*, Microstructures and properties of friction stir welded 304 austenitic stainless steel, Welding International, vol. 19, no 11, p. 877-881, nov. 2005, doi: 10.1533/wint.2005.3518.
[8] Sunilkumar, D., Muthukumaran, S., Vasudevan, M., & Reddy, M. G. (2020). Effect of friction stir and activated-GTA welding processes on the 9Cr–1Mo steel to 316LN stainless steel dissimilar weld joints. Science and Technology of Welding and Joining, 25(4), 311-319.
[9] Sunilkumar, D., Mathew, J., Muthukumaran, S., & Vasudevan, M. (2020). Friction Stir Welding of 2.25 Cr–1Mo Steel to AISI 316LN Stainless Steel. Transactions of the Indian Institute of Metals, 73, 1689-1693.
[10] CERN 1002. Technical requirements for 1.4429 (X2CrNiMo17-13-3, AISI 316LN) stainless steel sheets / plates for ultra - high vacuum applications at CERN.
[11] S. H. C. Park, Y. S. Sato, H. Kokawa, K. Okamoto, S. Hirano, et M. Inagaki, « Rapid formation of the sigma phase in 304 stainless steel during friction stir welding », Scripta Materialia, vol. 49, no 12, p. 1175-1180, déc. 2003, doi: 10.1016/j.scriptamat.2003.08.022.
[12] J. W. Ekin, "Experimental techniques for low – temperature measurements", New York, Oxford University press, 2006
[13] Weiss, K., & Nyilas, A. (2006). Specific aspects on crack advance during J-test method for structural materials at cryogenic temperatures. Fatigue & Fracture of Engineering Materials & Structures, 29(2), 83-92.
[14] Morris, J. W. (1993). Steels: for low temperature applications. Encyclopedia of Advanced materials.
[15] Ritchie, R. O. (2011). The conflicts between strength and toughness. Nature materials, 10(11), 817-822.
[16] Aviles Santillana, I., et al., (2018). A comparative study of fracture toughness at cryogenic temperature of austenitic stainless steel welds. Journal of Materials Engineering and Performance, 27(4), 1995-2002.